Cell PRESS
Structure
Article

Interconversion of Two GDP-Bound Conformations and Their Selection in an Arf-Family Small G Protein

Hideyasu Okamura,[1,2,*] Masaki Nishikiori,[1] Hongyu Xiang,[1] Masayuki Ishikawa,[1] and Etsuko Katoh[1,*]
[1]Division of Plant Sciences, National Institute of Agrobiological Sciences, 2-1-2, Kannondai, Tsukuba, Ibaraki 305-8602, Japan
[2]Institute of Advanced Energy, Kyoto University, Gokasyo, Uji, Kyoto 611-0011, Japan
*Correspondence: hokamura@iae.kyoto-u.ac.jp (H.O.), ekatoh@nias.affrc.go.jp (E.K.)
DOI 10.1016/j.str.2011.04.007

SUMMARY

ADP-ribosylation factor (Arf) and other Arf-family small G proteins participate in many cellular functions via their characteristic GTP/GDP conformational cycles, during which a nucleotide*Mg^{2+}-binding site communicates with a remote N-terminal helix. However, the conformational interplay between the nucleotides, the helix, the protein core, and Mg^{2+} has not been fully delineated. Herein, we report a study of the dynamics of an Arf-family protein, Arl8, under various conditions by means of NMR relaxation spectroscopy. The data indicated that, when GDP is bound, the protein core, which does not include the N-terminal helix, reversibly transition between an Arf-family GDP form and another conformation that resembles the Arf-family GTP form. Additionally, we found that the N-terminal helix and Mg^{2+}, respectively, stabilize the aforementioned former and latter conformations in a population-shift manner. Given the dynamics of the conformational changes, we can describe the Arl8 GTP/GDP cycle in terms of an energy diagram.

INTRODUCTION

Proteins are intrinsically flexible and dynamic molecules, and, as such, their native structures are dynamic conformational ensembles. Therefore, the static three-dimensional coordinates of a protein structure often cannot fully account for its function because its dynamic characteristics, which if known in enough detail can be diagramed as a free-energy landscape, are also required (Frauenfelder et al., 1991; Henzler-Wildman and Kern, 2007). Particularly, for those proteins that undergo large conformational changes in order to function, an understanding of their dynamic characters is absolutely necessary. The small G proteins of the Ras superfamily (GTPases of 20–25 kDa) function by switching between an active GTP-bound conformation that can bind an effector and an inactive GDP-bound conformation (GTP/GDP cycle) (Wennerberg et al., 2005; Colicelli 2004). Ras-family proteins have similar GTP-bound conformations (GTP form), in which a conserved Thr in the so-called switch I and a conserved Gly in the so-called switch II bind to the GTP γ-phosphate via their main-chain amide protons (Vetter and Wittinghofer, 2001) (Figure 1). Additionally, for all Ras-family proteins, when GTP is hydrolyzed to GDP, the switches move away from the nucleotide binding site (Vetter and Wittinghofer, 2001) (Figure 1). In Ras-family proteins, the transition between the GTP- and GDP-bound conformations has been structurally characterized using mutants that are likely to mimic intermediate states in X-ray crystallography (Hall et al., 2002; Ford et al., 2005, 2006). Molecular dynamics simulations of the transitions have also been performed (Diaz et al., 1997; Ma and Karplus, 1997; Noé et al., 2005; Gorfe et al., 2008; Grant et al., 2009, 2010). Notably, Ras, even when complexed with a GTP or GTP analogs, equilibrates between at least two conformational states, which have been identified by ^{31}P NMR spectroscopy, and this dynamic equilibrium affects its functional behavior, e.g., effector binding or GTPase activity (Spoerner et al., 2001, 2004, 2007, 2010). However, Arf-family proteins, which form a Ras subfamily and are the subject of the work reported herein, in their GDP-bound conformations (GDP form), exhibit additional conformational alterations not found in other Ras-family proteins: the so-called interswitch region that is part of the central core domain β sheet is shifted in registry by two residues (the interswitch toggle) (Pasqualato et al., 2002) and the N-terminal helix that is free in the GTP form occupies a hydrophobic surface exposed by the movement of the interswitch (Pasqualato et al., 2002) (Figure 1).

Arf-family proteins are often found at a membrane interface, and participate in various cellular events, e.g., membrane trafficking and microtubule dynamics (D'Souza-Schorey and Chavier, 2006; Gillingham and Munro, 2007; Kahn et al., 2005, 2006). There, the characteristic GTP/GDP conformational cycle presents a functional feature. Many Arf-family proteins are myristoylated at the highly conserved position 2 Gly (see Figure S1 available online), and the N-terminal region, including the helix, participates in membrane association/dissociation events that are initiated by a bound nucleotide (Kahn et al., 1992). Additionally, N-terminal modifications, e.g., myristoylation and truncation of the helix alter the apparent GDP to GTP exchange rate constant, which affects the bound nucleotide equilibrium population (Randazzo et al., 1994, 1995; Franco et al., 1995). Finally, Mg^{2+}, which is found in the GTP form and, in many cases, also in the GDP form (Figure 1), alters the GDP to GTP exchange rate constant (Franco et al., 1995; Ménétrey et al., 2000). Such regulatory mechanisms likely are correlated

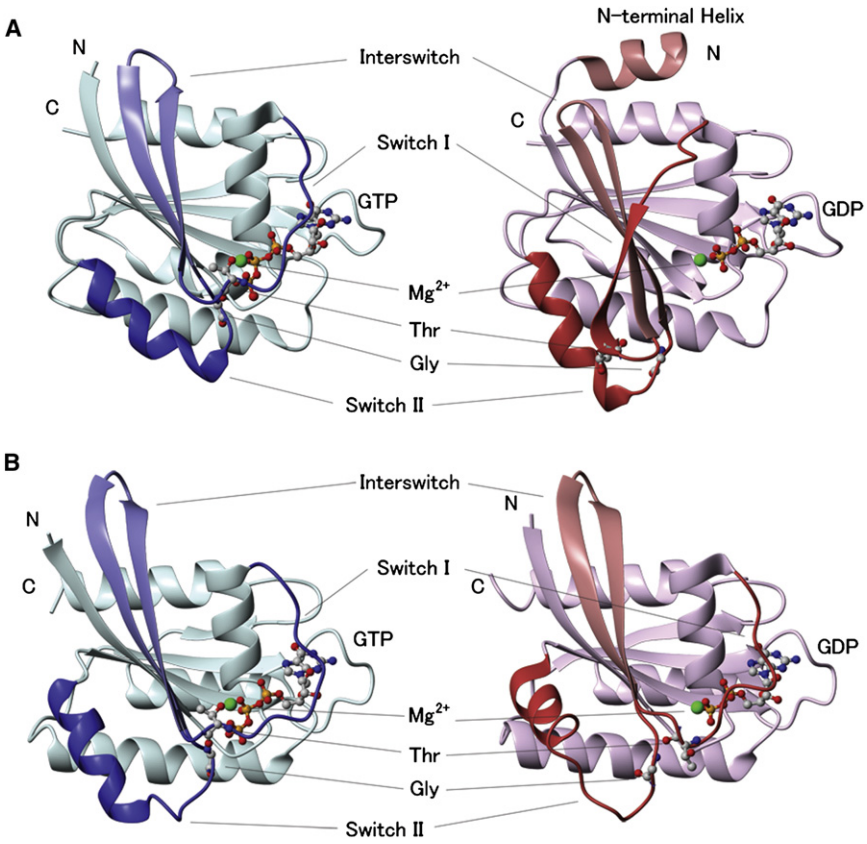

Figure 1. Structures of Arf6 and Ras with GTP or GDP Bound

(A) The crystal structures of human Arf6, a member of the Ras subfamily Arf, in complex with GTP (left; PDB accession number 2J5X) for which the 10 N-terminal residues are invisible, and with GDP (right; PDB accession number 1E0S) for which the N-terminal helix is bound to the core domain.

(B) The crystal structures of human Ras in complex with GTP (left; PDB accession number 5P21) and GDP (right; PDB accession number 4Q21). In each panel, switch I, switch II, the interswitch, and, for Arf6, the N-terminal helix are chromatically highlighted. The bound nucleotides and the conserved Gly and Thr residues that interact with the GTP γ-phosphate are shown as ball-and-stick representations. Mg^{2+} ions (in 1E0S, modeled as NH_4^+) are shown as green spheres. The information in this figure is supported by Figure S1.

with the internal dynamics of the proteins (Buosi et al., 2010). However, to date, how the bound nucleotides, the helix, Mg^{2+}, the core domain and effectors affect the overall conformational changes has not been examined in detail. For this study, we examined the dynamic characteristics underlying the conformational changes in an Arf-family protein, *Nicotiana tabacum* Arl8 (*Nt*Arl8), using NMR relaxation spectroscopy. Our results provide a dynamic view of the molecular mechanism for the GTP/GDP cycle of Arf-family proteins that incorporates the population-shift (pre-existing equilibrium) model for protein-ligand binding (see below).

RESULTS

An Mg^{2+}-Dependent Conformational Transition

Arl8 is conserved in most species, including humans, plants, and protista, which indicates that it is an ancient small G protein (Li et al., 2004). *Nt*Arl8 is 65% identical in sequence and 85% similar in sequence to human Arl8 (*Hs*Arl8) (Figure S1), for which three (unpublished) crystal structures complexed with GDP have been deposited into the Protein Data Bank: an N-terminally 8-residue-truncated Arl8 with the N-terminal helix (residues 9–17 according to the *Hs*Arl8a numbering sequence) bound to the core domain (Δ8*Hs*Arl8a-GDP, PDB accession number 2H18) and two N-terminally 17-residue-truncated Arl8s, for which the N-terminal helix had been removed (Δ17*Hs*Arl8a-GDP, PDB accession number 1ZD9; and Δ17*Hs*Arl8b-GDP, PDB accession number 2AL7). The crystal structures of the complexes appear to depend on the presence or absence of the N-terminal helix (Figure 2). The Δ8*Hs*Arl8a-GDP structure is typical of a GDP form that has undergone the interswitch toggle and N-terminal helix capping, whereas the structures of both Δ17*Hs*Arl8-GDPs have GTP-like conformations (GTP-like form) with the interswitch toggle positioned as in the GTP form. Additionally, Mg^{2+} was not found in its canonical binding site adjacent to GDP in Δ8*Hs*Arl8a-GDP, whereas, it was present in the Δ17*Hs*Arl8-GDP structures (Figure 2A). The Arf-family protein, *Mm*Arl3 also does not contain Mg^{2+} when in its GDP form (Hillig et al., 2000), and, in both cases, the absence of Mg^{2+} is probably due to the presence of a basic residue near the canonical Mg^{2+}-binding site (Lys 54 in *Mm*Arl3 and Arg58 in *Hs*Arl8), instead of the glutamate found in many other Arf-family proteins (Figure 2B; Figure S1).

Removal of the N-terminal helix from an Arf-family protein probably represents a state that has a conformation that is intermediate between those of the GTP- and GDP-bound forms and would therefore possibly mimic a state associated with the transition pathway of the membrane-bound GDP complex in vivo (Pasqualato et al., 2002). Therefore, the conformational transition between the two *Hs*Arl8 crystal structures is relevant to the functioning of Arf-family proteins. For the work reported herein, we used two derivatives of Arl8, N-terminally 7- and 16-residue-truncated *Nt*Arl8s (Δ7*Nt*Arl8 and Δ16*Nt*Arl8, respectively), designed to mimic the *Hs*Arl8 crystal structures (Figure S1). First, we characterized the secondary and tertiary structural elements of Δ16*Nt*Arl8-GTP that had been purified in the presence of GTP and Mg^{2+} by identifying the associated NOEs and confirmed that it was a typical GTP form (Figure S2D). Next, we determined the rate constant for the spontaneous hydrolysis of GTP by Δ16*Nt*Arl8-GTP·Mg^{2+} at 25°C ($1.14 \pm 0.08 \pm 10^{-5}$ s^{-1}), by monitoring, in real-time, its ^{1}H-^{15}N HSQC spectrum (data not shown). Unexpectedly, the spectrum of Δ16*Nt*Arl8-GDP that appeared during the GTP hydrolysis experiment had two sets of signals,

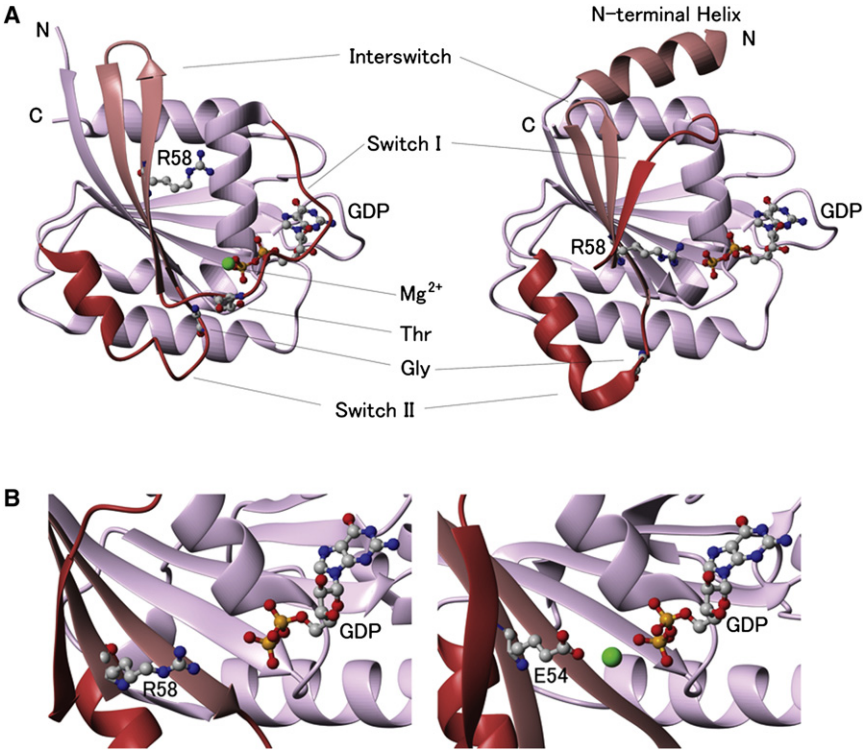

Figure 2. *Hs*Arl8 Structures

(A) Crystal structures of Δ17*Hs*Arl8a-GDP·Mg^{2+} (left: PDB accession number 1ZD9) and Δ8*Hs*Arl8a-GDP (right: PDB accession number 2H18).

(B) Comparison of the Mg^{2+} binding sites adjacent to the GTP γ-phosphate in *Hs*Arl8a (left: PDB accession number 2H18) and human Arf1 (right: PDB accession number 1HUR). In Arf1, Glu54 in the interswitch interacts with Mg^{2+}. In Arl8, Arg58 replaces Glu54 and would interact unfavorably with Mg^{2+}. For all panels, switch I, switch II, the interswitch, and the N-terminal helix are chromatically highlighted. The nucleotides, and the conserved Gly and Thr residues that interact with the GTP γ-phosphate are shown as ball-and-stick representations. Mg^{2+} ions are shown as green spheres. The information in this figure is supported by Figures S1 and S2.

and we subsequently found that the peak intensity ratios depended on the Mg^{2+} concentration. In the absence of Mg^{2+}, most of the residues produced only a single set of signals, although many of the signals for the residues in the two switches and neighboring regions were broadened or missing. When Mg^{2+} was added, many of the original signals decreased in intensity and many new signals emerged (Figure 3A; Figure S3A). At 30 mM Mg^{2+}, a new set of signals for almost all of the residues had appeared and those present in the spectrum of the 0 mM Mg^{2+} sample that were not part of this new set had nearly disappeared. We then characterized the solution structure of Δ16*Nt*Arl8-GDP in the presence of 30 mM Mg^{2+}, in terms of its secondary and tertiary structural elements, and confirmed that it is a GTP-like form, for which the interswitch maintained a GTP-like conformation; i.e., it was similar to the crystal structures of the Δ17*Hs*Arl8-GDPs (Figure S2C). Similarly, the ^{1}H-^{15}N HSQC spectrum of Δ7*Nt*Arl8-GDP in the absence of Mg^{2+} was similar to that of Δ16*Nt*Arl8-GDP in the absence of Mg^{2+} and, again, many of the signals associated with the residues in the two switches and neighboring regions were broadened or missing. *Nt*Arl8 also has an arginine (Arg57) at the position corresponding to Arg58 of *Hs*Arl8s, so that Mg^{2+} is probably not present in the GDP form of *Nt*Arl8. By identifying the appropriate NOE cross-peaks, we confirmed that the interswitch had toggled in Δ7*Nt*Arl8-GDP and in Δ16*Nt*Arl8-GDP when Mg^{2+} was not present (Figures S2A and S2B). In addition, the differences in their ^{1}H-^{15}N HSQC spectra may be ascribed to the presence or absence the N-terminal helix (Figures S3D and S3E). Therefore, the spectra of Δ7*Nt*Arl8-GDP and Δ16*Nt*Arl8-GDP, when Mg^{2+} was not included in the sample solution, are those typical of an Arf-family GDP form, i.e., like that of the Δ8*Hs*Arl8-GDP crystal structure. Unlike the spectral changes observed for Δ16*Nt*Arl8-GDP when Mg^{2+} was present, Mg^{2+} had little effect on the spectrum of Δ7*Nt*Arl8-GDP; only signals for some of the residues near the GDP-binding site had slightly shifted and/or were broadened (Figure 3A). Therefore a transition to a GTP-like conformation did not occur for Δ7*Nt*Arl8 in the presence of Mg^{2+}. In summary, the conformation of Δ16*Nt*Arl8-GDP reversibly changes between a GTP-like form and a GDP form, and the equilibrium depends on the Mg^{2+} concentration, whereas, Δ7*Nt*Arl8-GDP maintains the GDP form even in the presence of Mg^{2+}.

Core Domain Internal Dynamics

Two models, induced-fit (Koshland, 1958) and population-shift (pre-existing equilibrium) (Ma et al., 1999), have been proposed to account for the conformational changes that occur upon protein-ligand binding. The induced-fit model, which suggests that the initial, transient interaction between a protein and its ligand induces a conformational change that results in a more stable complex, has often been intuitively accepted. However, recent studies that have probed the dynamics of protein-ligand binding have indicated that the population-shift model, for which a protein equilibrates among thermally accessible conformations and the ligand selectively binds to one of these conformations, is more-widely applicable (Boehr et al., 2009). To clarify why the conformations of Δ7*Nt*Arl8-GDP and Δ16*Nt*Arl8-GDP responded differently to Mg^{2+}, we performed NMR R_2 relaxation dispersion experiments using samples of Δ7*Nt*Arl8-GDP and Δ16*Nt*Arl8-GDP that did not contain Mg^{2+} at 25°C. This type of NMR experiment probes the dynamics of a macromolecule on the μs-ms timescale and can discern sparsely populated substates (~1%) that are usually otherwise invisible (Loria et al., 1999; Mulder et al., 2001). The R_2 relaxation dispersion profiles differed substantially for the two *Nt*Arl8-GDP derivatives (Figure 3B). For Δ7*Nt*Arl8-GDP, the R_2 values for all available residues, excluding those in the loop region that connects the

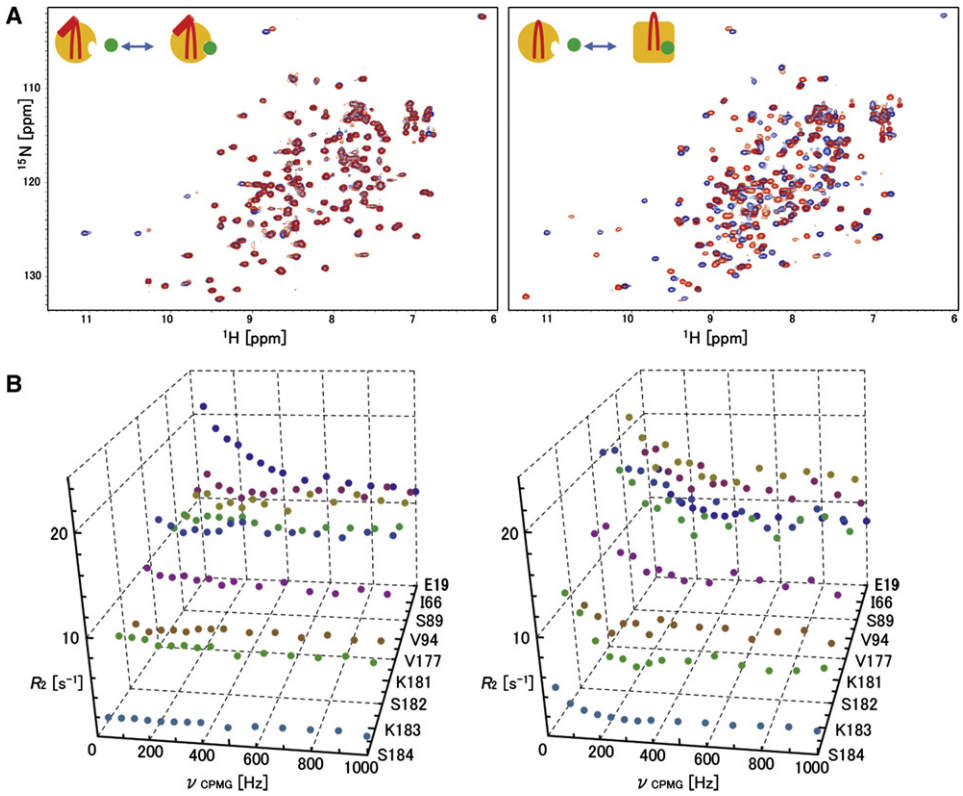

Figure 3. NMR Comparison of Δ7*Nt*Arl8-GDP and Δ16*Nt*Arl8-GDP

(A) ^{1}H-^{15}N HSQC spectra at 25°C of ^{15}N-labeled Δ7*Nt*Arl8 with GDP bound (left) and ^{15}N-labled Δ16*Nt*Arl8 with GDP bound (right). Each panel shows two spectra, one acquired for a sample in the absence of $MgCl_2$ (blue) and a second acquired for a sample that contained 10 mM $MgCl_2$ (red). Additionally, diagrams of the Mg^{2+} concentration-dependent conformational changes in *Nt*Arl8 are shown (see text), with the N-terminal helix for Δ7*Nt*Arl8, the interswitch regions, Mg^{2+}, and the core domains including the GDPs colored red, red, green, and orange, respectively. The GDP and GTP-like forms of the core domains are represented as circles and squares, respectively.

(B) ^{15}N R_2 relaxation dispersion profiles on the 600 MHz ^{1}H Larmor frequency at 25°C for representative residues of Δ7*Nt*Arl8-GDP (left) and Δ16*Nt*Arl8-GDP (right) when Mg^{2+} was not included in the samples. The information contained in this figure is supported by Figures S2 and S3.

N-terminal helix and the core domain (residues 19–20), were unaffected by ν_{CPMG}, which indicated that there were no large conformational fluctuations in the core domain on the order of μs to ms, except in two switch regions, for which many of the associated residues' R_2 profiles were not available. Conversely, the R_2 relaxation experiments indicated that a considerable number of the Δ16*Nt*Arl8-GDP residues' R_2 values varied significantly with increasing ν_{CPMG}. We fit the R_2 profiles for all observable Δ16*Nt*Arl8-GDP residues to a two-state model using the same kinetic parameters. Except for the χ^2 values (see Supplemental Experimental Procedures) for residues 35, 37, 39, 40, and 45, which are in switch 1 (residues 42–53) or in the helix (residues 31–41) that precedes switch 1, the χ^2 values for all other residues were similar and small (Figure 4B) which indicates that use of a global two-state model is generally correct. However, because many of the signals for the switch 1 residues were broadened or missing, that region of Δ16*Nt*Arl8-GDP seems to be highly mobile on the μs-ms time scale, which would affect the corresponding and neighboring residues' R_2 values. Therefore, the relevant residue R_2 values might not be fit by the model. The amide ^{15}N chemical shift differences derived from the R_2 measurements and those of most of the signals measured in the HSQC spectra of Δ16*Nt*Arl8-GDP in 0 versus 30 mM Mg^{2+} (GDP form and GTP-like form, respectively) are closely correlated, with a few exceptions, e.g., residue 45 (0.71 versus 2.95 ppm) (Figure 4C). Therefore, the R_2 profiles indicated that Δ16*Nt*Arl8-GDP equilibrated between two forms, most likely the GDP (92%) and GTP-like forms (8%). The rate constant for the GDP form to GTP-like form transition is 6.82 ± 1.87 s^{-1} and that for the GTP-like to GDP form transition is 82.23 ± 16.41 s^{-1} (Figure 4 and Table 1; Figure S4 and Table S1).

The R_2 relaxation dispersion experiments indicated that, most likely, the GTP-like form for Δ16*Nt*Arl8-GDP existed even in the absence of Mg^{2+}. However, because the GTP-like form was sparsely populated and because its signals were broadened by chemical exchange, it would have been very difficult to directly use its signals for exchange measurements. However, a signal associated with the minor form of Δ16*Nt*Arl8-GDP could be assigned to Ser184 in a ^{1}H-^{15}N HSQC spectrum in the absence of Mg^{2+}. This signal was sharp and strong, and was observed at a position almost identical to that of the Δ16*Nt*Arl8-GDP GTP-like form in the presence of Mg^{2+} (Figure S5A). We measured the exchange rates for the isolated major and minor Ser184 signals, using ZZ-exchange spectroscopy,

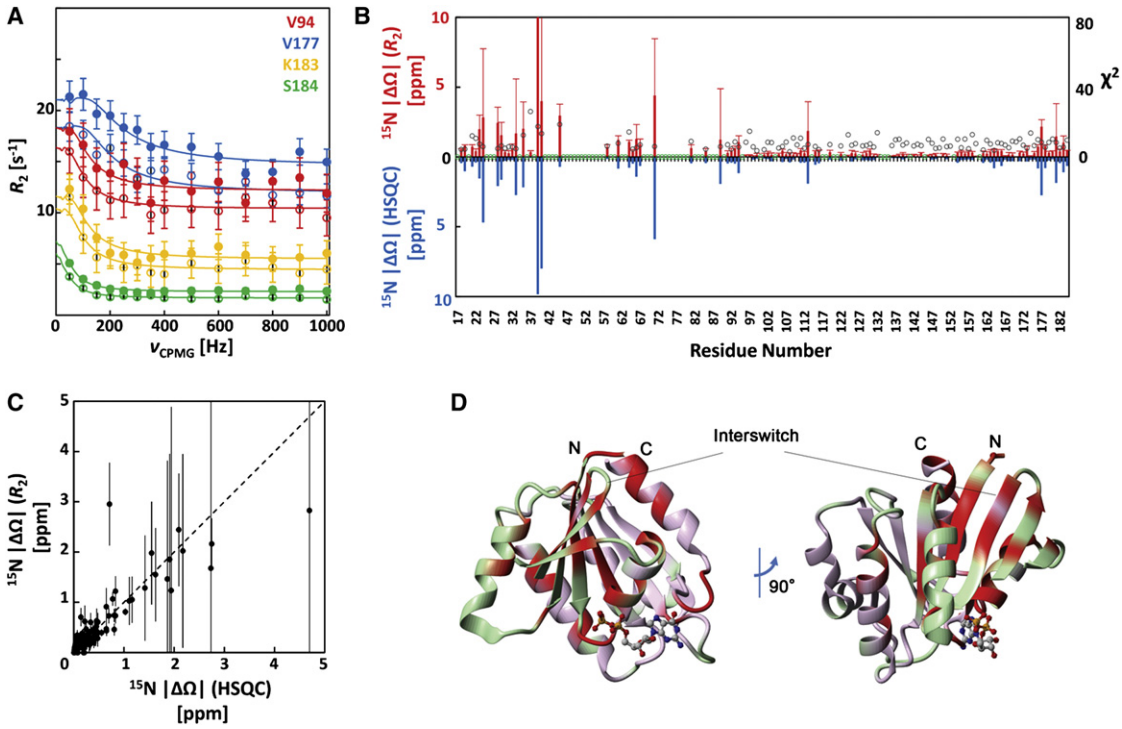

Figure 4. Model Fits of ^{15}N R_2 Relaxation Dispersion Profiles for Δ16*Nt*Arl8-GDP

(A) Examples of global two-state fits for the ^{15}N R_2 relaxation dispersion profiles on the 600 (filled circles) and 500 (open circles) MHz ^{1}H Larmor frequencies at 25°C for a sample of Δ16*Nt*Arl8-GDP that did not include Mg^{2+}. The fits used the global kinetic parameters and, residue-specific chemical-shift difference parameters. The errors in the peak intensities were calculated using duplicated data.

(B) Comparison of the absolute values of the amide ^{15}N chemical shift differences (ΔΩ) derived from the R_2 relaxation dispersion data (top) and those derived from the absolute values of the amide ^{15}N chemical shift differences for the GDP (0 mM Mg^{2+}) and GTP-like forms (30 mM Mg^{2+}) of Δ16*Nt*Arl8-GDP measured using ^{1}H-^{15}N HSQC spectra (bottom). The open black circles are the residue-specific χ^2 values obtained from the global fits. The green circles at the base of the x axis identify those residues for which ΔΩ values were not obtained because the signals overlapped, were broadened, or were missing. The error bars in the chemical shift differences derived from the R_2 relaxation dispersion data were estimated by Monte Carlo simulations.

(C) Correlation of the two sets of amide ^{15}N chemical shift differences given in (B). The error bars in the chemical shift differences derived from the R_2 relaxation dispersion data were estimated by Monte Carlo simulations.

(D) The chemical shift differences derived from the R_2 relaxation dispersion data are mapped onto the GDP form of Δ16*Nt*Arl8-GDP, the structure for which was build using MODELER (Sali and Blundell, 1993) (see Experimental Procedures for more details). Residues with chemical shift differences >0.4 ppm are colored red, and those for which data could not be obtained are colored pale green. The information contained in this figure is supported by Figure S4 and Table S1.

which can detect exchange rates on the ms time scale (Farrow et al., 1994). After fitting the ZZ-exchange data to a two-state model, the rate constants were found to be: for the main peak to the minor peak transition, 8.45 ± 1.17 s^{-1}, and for the minor peak to the major peak transition 83.64 ± 12.39 s^{-1} (Figure 5; Table 1). These rate constants are the same as those calculated for the R_2 measurements within experimental error. Therefore, the minor peak of Ser184 in the Δ16*Nt*Arl8-GDP ^{1}H-^{15}N HSQC spectrum under Mg^{2+}-free conditions is that of the GTP-like form.

These results strongly suggested that the conformational changes between the GDP and GTP-like forms of Δ16*Nt*Arl8-GDP are consistent with the pre-existing equilibrium model. If so, Mg^{2+} should increase the stability of only the GTP-like form. In the presence of 1 mM Mg^{2+}, signals from both the GDP and GTP-like forms, in addition to those of Ser184, in the ^{1}H-^{15}N HSQC spectrum of Δ16*Nt*Arl8-GDP were observable (Figure S3A). Using ZZ-exchange spectroscopy, we determined the exchange rate constants using the intensities of the Ser184 signals of a sample of Δ16*Nt*Arl8-GDP that contained 1 mM Mg^{2+} (Figure S5A) and found the rate constants to be 7.12 ± 0.31 s^{-1} and 11.78 ± 0.82 s^{-1} for the GDP form to GTP-like form and the GTP-like form to GDP form transitions, respectively (Figure 5 and Table 1). Therefore, Mg^{2+} clearly bound to the GTP-like form because a significant decrease in the rate constant for the GTP-like form to the GDP form transition was found. It is also reasonable to conclude that the GTP-like form of Δ7*Nt*Arl8-GDP is thermally inaccessible because Mg^{2+} did not affect the conformation of Δ7*Nt*Arl8-GDP.

Thermodynamic Parameters

Using transition-state theory (Laidler and King, 1983), the temperature dependences of the transition rate constants provide the activation thermodynamic parameters, $\Delta H^{\ddagger}$, $\Delta S^{\ddagger}$, and $\Delta G^{\ddagger}$. We acquired the temperature dependences of the transition rate constants for a sample of Δ16*Nt*Arl8-GDP that did not contain Mg^{2+} using the ZZ-exchange profiles of the Ser184 transitions (Table 1 and Figure 5; Figure S5B). The Eyring

Table 1. Conformational Transition Rate Constants and Mg^{2+} Association Constants

Temperature (°C)	0 mM $MgCl_2$		1 mM $MgCl_2$		
	$k_{GDP \rightarrow GTP\text{-}like}$ (s^{-1})	$k_{GTP\text{-}like \rightarrow GDP}$ (s^{-1})	$k_{GDP \rightarrow GTP\text{-}like}$ (s^{-1})	$k_{GTP\text{-}like \rightarrow GDP}$ (s^{-1})	$K_{A(Mg2+,\ GTP\text{-}like)}$ ($10^3\ M^{-1}$)
20 (R_2)	5.0 ± 2.5	56.7 ± 21.3			
25 (R_2)	6.8 ± 1.9	82.2 ± 16.4			
30 (R_2)	9.7 ± 1.2	135.5 ± 12.7			
10 (ZZ)	2.8 ± 0.3	12.8 ± 1.3	2.7 ± 0.2	4.1 ± 0.4	2.08 ± 0.41
15 (ZZ)	4.0 ± 0.3	21.6 ± 2.0	4.3 ± 0.2	6.3 ± 0.5	2.82 ± 0.44
20 (ZZ)	6.0 ± 0.7	45.4 ± 5.5	5.4 ± 0.2	9.3 ± 0.5	3.63 ± 0.67
25 (ZZ)	8.5 ± 1.2	83.6 ± 12.4	7.1 ± 0.3	11.8 ± 0.8	5.28 ± 1.15
30 (ZZ)			9.8 ± 0.8	24.3 ± 2.2	

R_2 and ZZ indicate that the rate constants for the conformational transitions of Δ16*Nt*Arl8-GDP, and the association constant for Mg^{2+} binding to the GTP-like form of Δ16*Nt*Arl8-GDP were obtained from the R_2 relaxation dispersion experiments and ZZ-exchange experiments, respectively. $k_{GDP \rightarrow GTP\text{-}like}$ and $k_{GTP\text{-}like \rightarrow GDP}$ are the rate constants for the GDP form to GTP-like form and the GTP-like form to the GDP form, respectively. $K_{A(Mg2+,\ GTP\text{-}like)}$ is the association constant for the binding of Mg^{2+} to the GTP-like form. The standard deviations in the transition rate constants were estimated by Monte Carlo simulations.

plots for both transitions were linear (Figure 6A). The values for $\Delta H^{\ddagger}$ and $\Delta S^{\ddagger}$ for the conversion of the GDP form to GTP-like form are 11.8 ± 1.8 kcal/mol and –14.6 ± 6.1 cal/mol·K, respectively, and those for the GTP-like form to GDP form transition are 20.6 ± 1.8 kcal/mol and 19.3 ± 6.3 cal/mol·K, respectively (Figure 6A). Using the values for $\Delta H^{\ddagger}$ and $\Delta S^{\ddagger}$, values for $\Delta G^{\ddagger}$ at 25°C were calculated as 16.2 ± 2.5 kcal/mol and 14.8 ± 2.6 kcal/mol for the GDP form to GTP-like form transition and the GTP-like form to GDP form transition, respectively. The energy diagram at 25°C (Figure 6A) indicates that the GDP form is entropically favored (ΔS) while the GTP-like form is enthalpically favored (ΔH). Signals of the GDP form switch regions of both Δ16*Nt*Arl8-GDP and Δ7*Nt*Arl8-GDP were broadened or missing, which indicates that these regions are mobile on the μs-ms time scale and the motions of these regions are not influenced by the N-terminal region. Therefore, the mobility of these regions may contribute to the favorable ΔS found for the GDP form. Although the values of ΔH and ΔS between the GDP and GTP-like forms differ substantially (Figure 6A), they offset each other, so that the value for ΔG is small.

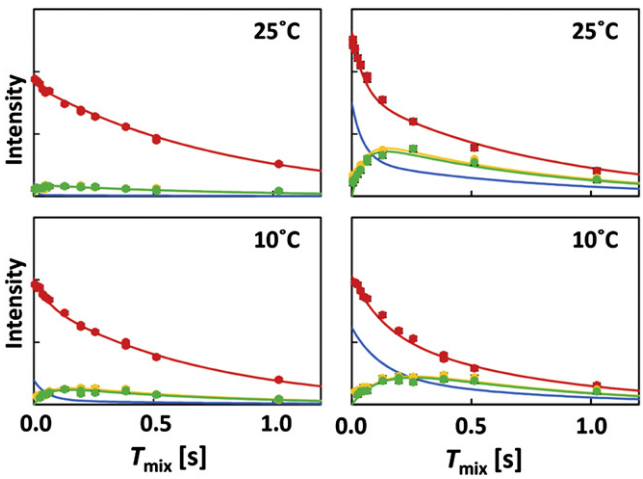

Figure 5. NMR ZZ-exchange Profiles for Δ16*Nt*Arl8-GDP S184

ZZ-exchange peak intensity profiles for the signals of Δ16*Nt*Arl8-GDP S184 at 25°C (top) or 10°C (bottom) for samples that contained 0 mM (left) or 1 mM $MgCl_2$ (right). Red data points are the autopeak intensities of the GDP form. Green and orange data points are the cross-peak intensities for the GTP-like form to GDP form and GDP form to GTP-like form transitions, respectively. Because of the overlap with another resonance, the autopeak intensities of the GTP-like form Ser184 were not measured. The exchange rate constants for transitions were obtained by a two-state fit that used the values of the three peak intensity data sets. The blue line in the bottom plot is the calculated curve expected for the autopeak intensities of the GTP-like form. The information contained in this figure is supported by Figure S5. The errors in the peak intensities were calculated using duplicated data.

We also examined the temperature dependences of the rate constants for the conformational transitions of Δ16*Nt*Arl8-GDP in the presence of 1 mM Mg^{2+} (Table 1 and Figure 5; Figure S5). At all measured temperatures, the rate constants for the GDP form to GTP-like form transition were almost the same as those found when Mg^{2+} was not present, whereas, those for the GTP-like form to GDP form transition were significantly smaller than when Mg^{2+} was not present. In addition, the Eyring plots showed that the value for the slope of the GTP-like form to the GDP form transition decreased when Mg^{2+} was included in the sample (Figure S5A), which indicated that the value of $\Delta H^{\ddagger}$ was smaller and that the binding of Mg^{2+} to the GTP-like form is an enthalpically unfavorable process. Knowing that Mg^{2+} binds to the GTP-like form of Δ16*Nt*Arl8-GDP, we could calculate the GTP-like form/Mg^{2+} temperature-dependent association constants (K_A) and use them to generate the van't Hoff plot of Figure 6B so that the thermodynamic parameters for Mg^{2+} binding to the GTP-like form could be determined. The values are ΔH° = 10.1 ± 3.07 kcal/mol and ΔS° = 50.9 ± 10.3 cal/mol·K (Figure 6B). Therefore, the thermodynamic parameters of the Mg^{2+}-dependent conformational transitions can be divided into contributions from the intrinsic conformational transitions and the binding of Mg^{2+} to the pre-existing GTP-like form.

DISCUSSION

During the GTP/GDP cycles of the Arf-family proteins, similar large conformational changes that involve the interswitch toggle

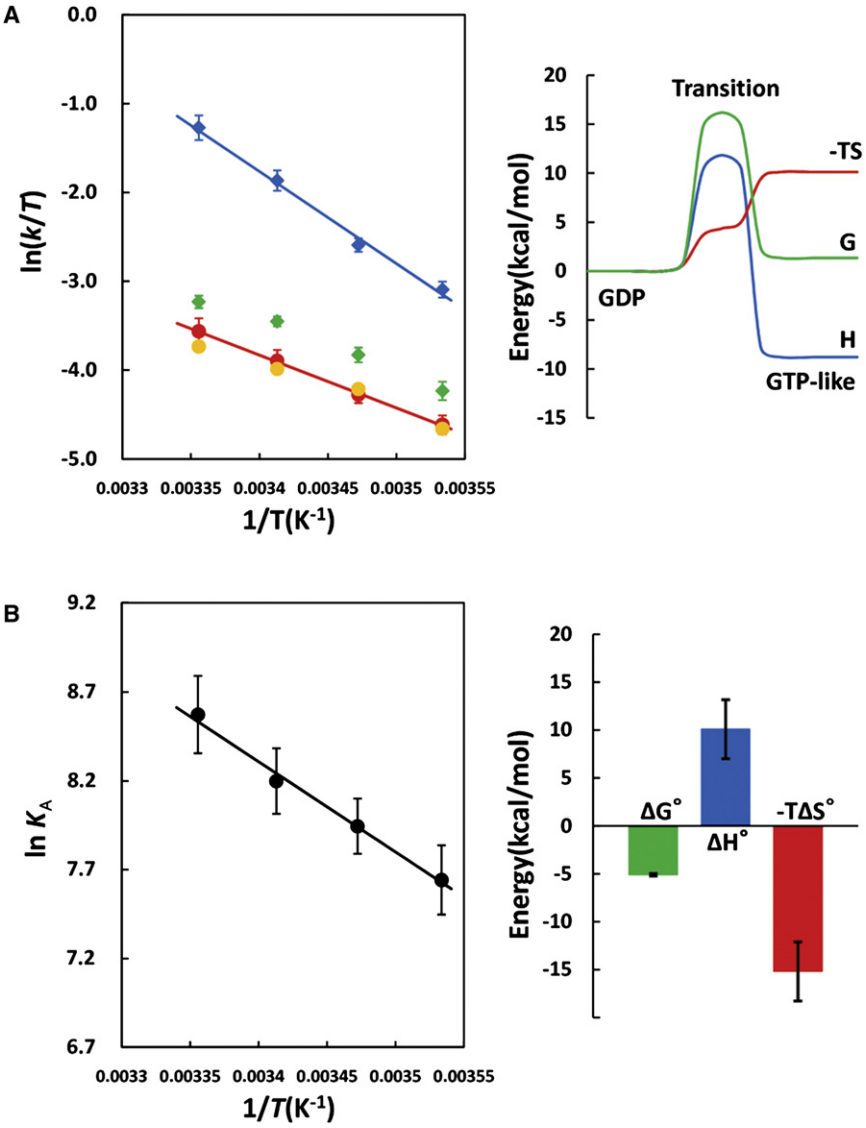

Figure 6. Thermodynamic Characterization of the Δ16*Nt*Arl8-GDP Conformational Transition and the Binding of Mg^{2+} to the GTP-like Form of Δ16*Nt*Arl8-GDP

(A) Eyring plots for the GDP form to GTP-like form transition (red and orange) and for the GTP-like form to GDP form transition (blue and green) for samples that did not (red and blue) and did (orange and green) contain 1 mM $MgCl_2$. The corresponding energy diagram is for the Δ16*Nt*Arl8-GDP sample at 25°C that did not contain Mg^{2+}.

(B) A van't Hoff plot and an energy diagram for the binding of Δ16*Nt*Arl8-GDP and Mg^{2+} at 25°C. The rate constants used to calculate the temperature-dependent association constants (K_A) were those for the GDP form/GTP-like form transitions obtained using samples that did and did not contain 1 mM Mg^{2+}. The error bars in the energy diagram were estimated by Monte Carlo simulations.

and N-terminal helix capping occur, which do not occur during the cycles of other Ras superfamily proteins (Pasqualato et al., 2002). We demonstrated that the core domain of *Nt*Arl8 (Δ16*Nt*Arl8), when complexed with GDP, equilibrates between two conformations: the GDP form in which the interswitch has toggled and the GTP-like form in which the interswitch is positioned similarly to that of the GTP form, but the conformations of the switch regions are different as a result of the presence or absence of the GTP γ-phosphate. The N-terminal helix and Mg^{2+} stabilize the GDP and GTP-like forms, respectively, in ways that are consistent with the population-shift model. Unlike many other Arf-family proteins, *Nt*Arl8, when in the GDP form, does not appear to bind Mg^{2+}. We could therefore use Mg^{2+} as a probe for the GTP-like form. We expect that Mg^{2+} stabilizes the GDP forms and the (putative) GTP-like forms of many Arf-family proteins (Figure S6), and it is therefore probable that the conformations of the Arf-family proteins when bound to GDP are governed by both the N-terminal helix, which stabilizes the GDP form and Mg^{2+}, which stabilizes both the GDP and GTP-like forms, although the relative populations of the two conformations will vary somewhat. It is interesting that EDTA or disturbing the GDP form Mg^{2+}-binding site increased the rate of the GDP to GTP exchange in Δ17Arf1-GDP (Ménétrey et al., 2000). In addition, it has recently been reported that the GDP form for Δ17Arf1-GDP also fluctuated on the μs-ms time scale, although the presence of a GTP-like form was not recognized and characterized (Buosi et al., 2010) as we have done for *Nt*Arl8. The authors of that study performed amide ^{15}N R_2 relaxation dispersion experiments using Δ17Arf1-GDP, and found significant dispersion profiles for residues throughout the molecule. However, the authors did not determine the populations of the major and minor states and the chemical shift difference for each residue in the two states because they used an approximated two-state fast exchange limit function (Luz and Meiboom, 1963) for which the parameters for the populations and for the chemical shift differences could not be derived. In addition, although the authors obtained a relative value for each chemical shift difference by using a fixed major and minor population ratio, unlike those for Δ16*Nt*Arl8, the chemical shift values for the residues of the putative GTP-like form of Δ17Arf1-GDP were not measured which means that the validity of the values of the chemical shift differences obtained from the R_2 relaxation profiles have not been quantitatively verified by other means although H-D exchange experiments revealed that the interswitch region was mobile. However, because the distribution of residues exhibiting significant dispersion profiles in Δ17Arf1-GDP resembles that found for Δ16*Nt*Arl8-GDP, it may be that the minor state in Δ17Arf1-GDP also corresponds to a GTP-like form that has fully experienced the interswitch toggle. The exchange rate constant between the major and minor

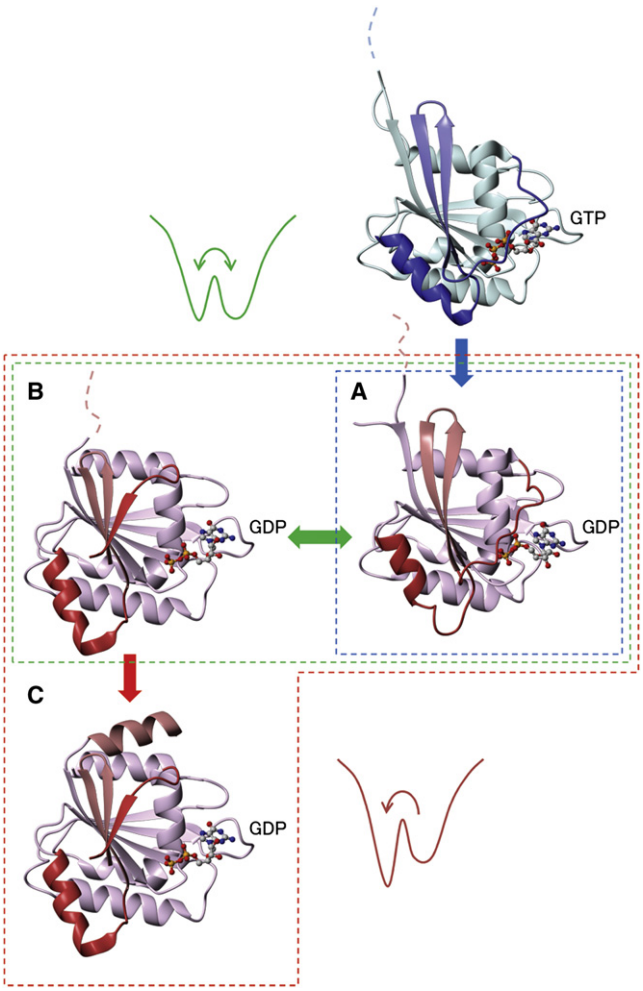

Figure 7. The *Nt*Arl8 Conformational Transitions and the Associated Energy Diagrams

The conformations of the GTP and GDP complexes are colored blue and red, respectively. The conformational state of the interswitch distinguishes the structures on the right from those on the left. The three GDP complexes are (A) the GTP-like form and the GDP form (B) before and (C) after N-terminal capping. The blue, green, and red double-headed arrows indicate the hydrolysis of GTP, the interswitch toggle, and capping of the N-terminal helix, respectively. Structures within the red, green, and blue broken lines represent the allowed conformational space for Δ7*Nt*Arl8-GDP, Δ16*Nt*Arl8-GDP, and Ras superfamily proteins that do not undergo an interswitch toggle, respectively. The energy diagrams for the conformational transitions of Δ7*Nt*Arl8-GDP and Δ16*Nt*Arl8-GDP are shown in red and green, respectively. The *Nt*Arl8 structural coordinates for the GTP- and GTP-like forms were obtained using Cyana (Güntert et al., 1997; Herrmann et al., 2002) and the NMR structural data, and the GDP forms were built using MODELER (Sali and Blundell, 1993) (see Experimental Procedures for more detail).

states for Δ17Arf1-GDP (k_{ex} = 1530 ± 110 S^{-1} at 25°C) is much faster than that found for Δ16*Nt*Arl8-GDP (k_{ex} ($k_{GDP \rightarrow GTP\text{-}like}$ + $k_{GTP\text{-}like \rightarrow GDP}$) = 89.0 ± 16.5 S^{-1} at 25°C), which may be a consequence of the truncation-site positions. Residue 1 of Arf1 corresponds to residue 3 of *Nt*Arl8 and thus, the first two residues of the first β strand are missing in Δ17Arf1 (Figure S1), which may destabilize the GTP-like form of Δ17Arf1-GDP. Notably, considerable differences in the GDP dissociation rate constants for Δ13Arf1 and Δ17Arf1 have been measured (Randazzo et al., 1994, 1995), and, as mentioned above, the concentration of Mg^{2+} also affects the transition rates more drastically for Arf1 than it does for *Nt*Arl8.

The Arl8 energy diagrams described herein may be characteristic of those for Arf-family proteins in general. Figure 7 shows the conformational changes of *Nt*Arl8 before and after the interswitch toggle has occurred and the energy diagrams for the transitions when GDP is bound. For non-Arf-family proteins of the Ras superfamily, the interswitch toggle does not occur, which means that they probably maintain the GTP-like form discussed herein even when GDP is bound. The Ras-family GTP and GDP forms respectively represent a conformationally well-defined active form, which effectively binds an effector, and a relaxed inactive form (Vetter and Wittinghofer, 2001), although when GTP is bound, the switch regions of Ras equilibrate among multiple conformational states (Spoerner et al., 2010). When the GTP γ-phosphate is hydrolyzed, Ras transitions to the energetically more favorable GDP conformation (or to a conformational ensemble) that is unresponsive to an effector. Therefore, the energetic cost of maintaining the conformationally active form, i.e., when GTP is bound, may be used to regulate effector binding. Because the position of the Ras insterswitch that connects the two switch regions is the same in the two conformations, Ras seems to be restored to its GTP form simply by GDP/GTP exchange. Relevantly, a recent computational study showed that the nucleotide free states for both Ras and Rho (another subfamily member of the Ras superfamily) interconvert between conformations that resemble the GTP- and GDP forms, which suggests that the pre-existing equilibrium model is also the dominant mechanism for their nucleotide-dependent conformational transitions (Grant et al., 2010). For Arf-family proteins, furthermore, toggling of the interswitch, which involves rearrangement of the hydrogen bond network in the central β sheet, changes the conformations (or conformational ensembles) of the two switch regions. The toggled interswitch is then stabilized by the N-terminal helix. Therefore, to return to the GTP form, the interswitch must first be toggled to the GTP-like form before nucleotide exchange can occur (see below). However, because the activation barrier is high enough to inhibit the conversion of the GDP form to the GTP-like form, the GDP form can be distinguished from the GTP or GTP-like form (Figure 7). The Arf-family proteins, therefore, appear to be better organized molecular switches than are other members of the Ras superfamily. For Rho- or Rab-family proteins, which are two other subfamilies of the Ras superfamily, the GDP dissociation inhibitor (GDI) maintains their GDP-bound states and chaperones them into the cytosol (Jaffe and Hall, 2005; Stenmark, 2009). It is interesting that the Rho- or Rab-family proteins require GDIs to function; the GDIs seem to function as do the interswitch toggle and the N-terminal helix together (Figure 7).

The N-terminal helix is intimately involved in the GDP to GTP exchange process. Like other Arf-family proteins (Kahn et al., 1992; Ménétrey et al., 2000), Δ16*Nt*Arl8 spontaneously exchanges GDP for GTP ($\sim 10^{-3}$ s^{-1}), whereas, the exchange process is significantly slower for Δ7*Nt*Arl8 (Figure 8), which suggests that the GTP-like form must be present for the exchange process to occur. Typically, GDP/GTP nucleotide exchanges are stimulated by guanine nucleotide exchange

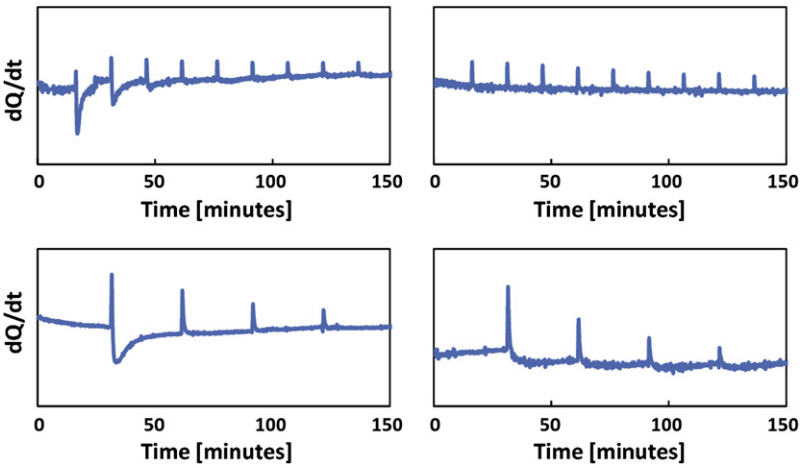

Figure 8. Isothermal Titration Calorimetry for GDP/GTP Exchange in *Nt*Arl8

The left and right panels show isothermal titration calorimetry tracings for the spontaneous exchange of GDP for GTP in Δ16*Nt*Arl8 and Δ7*Nt*Arl8, respectively. The experiments were performed at 25°C and used solutions of 50 μM Δ16*Nt*Arl8-GDP or Δ7*Nt*Arl8-GDP in 20 mM sodium phosphate (pH 7.0), 100 mM NaCl, 200 μM $MgCl_2$, and 1.25 mM GTP in the same buffer solution. The GTP solution (2 [top] or 8 μl [bottom]) was injected into the protein-GDP solution (200 μl) contained in the calorimeter sample cell. The gradual downward tracings (exothermic reaction) indicate that Δ16*Nt*Arl8 spontaneously exchanged GDP for GTP, whereas the nearly complete absence of such tracings indicated that Δ7*Nt*Arl8 did not exchange GDP for GTP. The sharp upward tracings (endothermic reactions) were caused by diluting the protein-GDP solution with the GTP solution.

factors (GEFs) (Gillingham and Munro, 2007; Casanova, 2007). However, to date, a GEF for Arl8 has not been found. Consideration of Arf1, for which the most structural detail is available (Amor et al., 1994; Greasley et al., 1995; Goldberg, 1998, 1999; Renault et al., 2003; Mossessova et al., 2003; Shiba et al., 2003; Liu et al., 2009, 2010), including myristoylated solution structures (Liu et al., 2009, 2010), is illuminating. Arf1 is stimulated by the sec7 domains of GEFs (Casanova, 2007). To date, three distinct crystal structures of Arf1-sec7 complexes, a brefeldin A (Donaldson et al., 1992; Peyroche et al., 1999) (BFA)-trapped Arf1-GDP-sec7 (Renault et al., 2003; Mossessova et al., 2003), a charge-reversal-trapped Δ17Arf-GDP-sec7(E156K) (Renault et al., 2003), and a nucleotide-free Δ17Arf1-sec7 (Goldberg, 1998), have been reported and are considered to represent three successive stages of the sec7-stiumulated nucleotide exchange process (Renault et al., 2003), which suggests that exchange occurs via the transient binding of sec7 to the GDP form, followed by an interswitch toggle to the GTP-like form, and, finally, GDP dissociation. Notably, these processes are similar to those required for the dissociation of GDP from Δ16*Nt*Arl8. The crystal structures of Arf1-GDP-sec7 complexed with the natural inhibitor BFA (Renault et al., 2003; Mossessova et al., 2003) are considered to be representative of the initial, transient Arf1-GDP-sec7 complex in which the interswitch toggle has not occurred (Béraud-Dufour et al., 1999). However, how a naturally occurring Arf1-GDP-sec7 transient complex, i.e., one that is formed in the absence of BFA but has the cavity that can be filled by BFA, could induce the subsequent interswitch toggle to stabilize the Arf1- sec7 interaction, has not been explained. An empty cavity caused by the absence of BFA is more likely to induce sec7 dissociation rather than toggling the interswitch. Additionally, sec7 hardly stimulates to myristoylated Arf1-GDP in the absence of membrane lipids (Chardin et al., 1996; Paris et al., 1997). However, using the pre-existing equilibrium model, a reasonable explanation can be offered. Assuming that the GDP-bound Arf1 core domain is thermally accessible to the GTP-like form, and that membrane lipids destabilize the N-terminal helix/core interaction and consequently the GDP form, then sec7 can more easily bind to the GTP-like form. Therefore, sec7 also may stabilize a pre-existing GTP-like form.

For this paper, we characterized the dynamics underlying the conformational changes in Arl8 and were therefore able to model the conformational changes that occur in Arf-family proteins and describe the associated energy diagrams. To date many studies have characterized Arf-family proteins according to how the two distinct conformations function. However, the functions of proteins depend on dynamic processes. Therefore, it is also important to delineate the conformational changes necessary for function.

EXPERIMENTAL PROCEDURES

NMR Peak Assignments and Structural Analysis

Δ7*Nt*Arl8 (residues 8–184) and Δ16*Nt*Arl8 (residues 17–184) were prepared as described in Supplemental Experimental Procedures. For peak assignment and structural analyses, NMR spectra were acquired at 25°C using Bruker 600 and 500 MHz spectrometers. Data were processed and analyzed using NMRPipe and NMRWish (Delaglio et al., 1995). The samples of Δ16*Nt*Arl8-GTP·Mg^{2+}, the GTP-like form of Δ16*Nt*Arl8-GDP (in the presence of Mg^{2+}), the GDP form of Δ16*Nt*Arl8-GDP (in the absence of Mg^{2+}), and Δ7*Nt*Arl8-GDP, each contained 0.2–0.3 mM ^{13}C,^{15}N-labeled protein in complex with a non-labeled nucleotide, 20 mM sodium phosphate (pH 7.0), 100 mM NaCl, 10% ^2H_2O. Additionally, 5 mM GTP and 5 mM $MgCl_2$ were present in the Δ16*Nt*Arl8·GTP·Mg^{2+} sample and 30 mM $MgCl_2$ was present in the sample of the GTP-like form of Δ16*Nt*Arl8-GDP. Although GTP in the Δ16*Nt*Arl8-GTP·Mg^{2+} sample was hydrolyzed to GDP, the initial 5 mM GTP concentration was sufficient to maintain the GTP-bound state of Δ16*Nt*Arl8 for ~10 days, which allowed us to acquire a series of spectra for Δ16*Nt*Arl8-GTP·Mg^{2+}. Backbone assignments for the resonances of all samples were obtained by conventional methods (Cavanagh et al., 2007). Additionally, for Δ16*Nt*Arl8-GTP·Mg^{2+} and the GTP-like form of Δ16*Nt*Arl8-GDP·Mg^{2+}, side-chain assignments were made, and solution structures were built using the usual structural information and Cyana (Güntert et al., 1997; Herrmann et al., 2002), which can automatically assign NOESY cross-peaks. Structures of Δ7*Nt*Arl8-GDP and the GDP form of Δ16*Nt*Arl8-GDP were built using MODELER (Sali and Blundell, 1993) and the crystal structure of Δ8*Hs*Arl8a-GDP (PDB accession number 2H18) as the template.

NMR R_2 Relaxation Dispersion Experiments

^{15}N R_2 relaxation dispersion (Loria et al., 1999; Mulder et al., 2001) data were acquired using Bruker 600 and 500 MHz spectrometers and the pulse sequence developed by Hansen et al. (2008), and samples that contained 0.18 mM Δ7*Nt*Arl8-GDP or Δ16*Nt*Arl8-GDP in 20 mM sodium phosphate (pH 7.0), 100 mM NaCl, 10% ^2H_2O. A constant relaxation delay time (T_{CP}) of 40 ms was used. The data for Δ16*Nt*Arl8-GDP were fit to a global two-state model (see Supplemental Experimental Procedures for more detail).

NMR ZZ-Exchange Experiments

ZZ-exchange (Farrow et al., 1994) data were acquired between 10 and 30°C with a Bruker 500 MHz spectrometer and solutions of 0.18 mM Δ16*Nt*Arl8-GDP in 20 mM sodium phosphate (pH 7.0), 100 mM NaCl, 10% ^2H_2O that contained 0 mM or 1 mM $MgCl_2$. The intensities of the S184 autopeak of the GDP form and the two cross-peaks arising from the GDP and GTP-like forms were used for the analysis. Mixing times (T_{mix}) of 4, 12, 24, 36, 48, 64, 128, 196, 256, 384, 512, and 1024 ms were used. The data were fit to a two-state exchange model (see Supplemental Experimental Procedures for more detail).

Thermodynamic Parameters for the Conformational Transitions and Mg^{2+} Binding

The activation enthalpies ($\Delta H^{\ddagger}$) and entropies ($\Delta S^{\ddagger}$) for interconversion between the GDP and GDP-like forms of Δ16*Nt*Arl8-GDP in the absent of Mg^{2+} were determined using the temperature dependencies of the rate constants (k) derived from the ZZ-exchange experiments and the Eyring equation as follows:

$$\ln\left(\frac{k}{T}\right) = -\frac{\Delta H^{\ddagger}}{R}\cdot\frac{1}{T} + \ln\left(\frac{k_B}{h}\right) + \frac{\Delta S^{\ddagger}}{R},$$

where T is the temperature, R is the gas constant, k_B is Boltzmann's constant, and h is Planck's constant. Errors associated with the parameters used in the fits were estimated by Monte Carlo simulations.

The temperature-dependent association constants (K_A) for Mg^{2+} bound to the GTP-like form were calculated using the rate constants for the GDP form and GTP-like form transitions that occurred in the absent and present of 1 mM $MgCl_2$, and with the assumption that Mg^{2+} interacted with only the pre-existing GTP-like form. The following equations were solved simultaneously for each temperature-dependent K_A:

$$K_A = \frac{[B\cdot Mg^{2+}]}{[B][Mg^{2+}]}$$

$$\frac{k_{AB,0}}{k_{BA,0}} = \frac{[B]}{[A]}$$

$$\frac{k_{AB,1}}{k_{BA,1}} = \frac{[B] + [B\cdot Mg^{2+}]}{[A]}$$

$$[P]_T = [A] + [B] + [B\cdot Mg^{2+}]$$

$$[Mg^{2+}]_T = [B\cdot Mg^{2+}] + [Mg^{2+}],$$

where A and B indicate the GDP and GTP-like forms, and $k_{AB,0}$, $k_{BA,0}$, and $k_{AB,1}$ and $k_{BA,1}$, are the transition rate constants for the GDP form/GTP-like form transitions in the absent and present of 1 mM $MgCl_2$, respectively, and [A], [B], [Mg^{2+}] and [B·Mg^{2+}] are the concentrations of the free GDP form, the free GTP-like form, free Mg^{2+}, and the GTP-like form/Mg^{2+} complex, respectively, and $[P]_T$ and $[Mg^{2+}]_T$ are the total concentrations of Δ16*Nt*Arl8·GDP and Mg^{2+}, respectively. For the binding of Mg^{2+} to the GTP-like form the association enthalpy (ΔH°) was calculated using the dependence of the K_As on temperature (the van't Hoff equation):

$$\frac{d(\ln K_A)}{d(1/T)} = -\frac{\Delta H^{\circ}}{R}$$

and the association entropy (ΔS°) using:

$$\Delta S^{\circ} = \Delta H^{\circ}/T + R\ln K_A,$$

where T is temperature, R is the gas constant. Errors associated with the parameters used in the fits were estimated by Monte Carlo simulations.

SUPPLEMENTAL INFORMATION

Supplemental Information includes Supplemental Experimental Procedures, six figures, and one table and can be found with this article online at doi:10.1016/j.str.2011.04.007.

ACKNOWLEDGMENTS

This work was supported by a grant from the program for promotion of basic and applied researches for innovations in Bio-oriented Industry (BRAIN).

Received: December 1, 2010
Revised: March 25, 2011
Accepted: April 1, 2011
Published: July 12, 2011

REFERENCES

Amor, J.C., Harrison, D.H., Kahn, R.A., and Ringe, D. (1994). Structure of the human ADP-ribosylation factor 1 complexed with GDP. Nature *372*, 704–708.

Boehr, D.D., Nussinov, R., and Wright, P.E. (2009). The role of dynamic conformational ensembles in biomolecular recognition. Nat. Chem. Biol. *5*, 789–796.

Buosi, V., Placial, J.P., Leroy, J.L., Cherfils, J., Guittet, É., and Van Heijenoort, C. (2010). Insight into the role of dynamics in the conformational switch of the small GTP-binding protein Arf1. J. Biol. Chem. *285*, 37987–37994.

Béraud-Dufour, S., Paris, S., Chabre, M., and Antonny, B. (1999). Dual interaction of ADP ribosylation factor 1 with Sec7 domain and with lipid membranes during catalysis of guanine nucleotide exchange. J. Biol. Chem. *274*, 37629–37636.

Casanova, J.E. (2007). Regulation of Arf activation: the Sec7 family of guanine nucleotide exchange factors. Traffic *8*, 1476–1485.

Cavanagh, J., Fairbrother, W.J., Palmer, A.G., III, Skelton, N.J., and Rance, M. (2007). Protein NMR Spectroscopy, Second Edition: Principles and Practice 2nd ed. (San Diego, CA: Academic Press).

Chardin, P., Paris, S., Antonny, B., Robineau, S., Béraud-Dufour, S., Jackson, C.L., and Chabre, M. (1996). A human exchange factor for ARF contains Sec7- and pleckstrin-homology domains. Nature *384*, 481–484.

Colicelli, J. (2004). Human RAS superfamily proteins and related GTPases. Sci. STKE *2004*, RE13.

Delaglio, F., Grzesiek, S., Vuister, G.W., Zhu, G., Pfeifer, J., and Bax, A. (1995). NMRPipe: a multidimensional spectral processing system based on UNIX pipes. J. Biomol. NMR *6*, 277–293.

Diaz, J.F., Wroblowski, B., Schlitter, J., and Engelborghs, Y. (1997). Calculation of pathways for the conformational transition between the GTP- and GDP-bound states of the Ha-ras-p21 protein: calculations with explicit solvent simulations and comparison with calculations in vacuum. Proteins *28*, 434–451.

Donaldson, J.G., Finazzi, D., and Klausner, R.D. (1992). Brefeldin A inhibits Golgi membrane-catalysed exchange of guanine nucleotide onto ARF protein. Nature *360*, 350–352.

D'Souza-Schorey, C., and Chavrier, P. (2006). ARF proteins: roles in membrane traffic and beyond. Nat. Rev. Mol. Cell Biol. *7*, 347–358.

Farrow, N.A., Zhang, O., Forman-Kay, J.D., and Kay, L.E. (1994). A heteronuclear correlation experiment for simultaneous determination of ^{15}N longitudinal decay and chemical exchange rates of systems in slow equilibrium. J. Biomol. NMR *4*, 727–734.

Ford, B., Skowronek, K., Boykevisch, S., Bar-Sagi, D., and Nassar, N. (2005). Structure of the G60A mutant of Ras: implications for the dominant negative effect. J. Biol. Chem. *280*, 25697–25705.

Ford, B., Hornak, V., Kleinman, H., and Nassar, N. (2006). Structure of a transient intermediate for GTP hydrolysis by ras. Structure *14*, 427–436.

Franco, M., Chardin, P., Chabre, M., and Paris, S. (1995). Myristoylation of ADP-ribosylation factor 1 facilitates nucleotide exchange at physiological Mg^{2+} levels. J. Biol. Chem. *270*, 1337–1341.

Frauenfelder, H., Sligar, S.G., and Wolynes, P.G. (1991). The energy landscapes and motions of proteins. Science *254*, 1598–1603.

Gillingham, A.K., and Munro, S. (2007). The small G proteins of the Arf family and their regulators. Annu. Rev. Cell Dev. Biol. *23*, 579–611.

Goldberg, J. (1998). Structural basis for activation of ARF GTPase: mechanisms of guanine nucleotide exchange and GTP-myristoyl switching. Cell *95*, 237–248.

Goldberg, J. (1999). Structural and functional analysis of the ARF1-ARFGAP complex reveals a role for coatomer in GTP hydrolysis. Cell *96*, 893–902.

Gorfe, A.A., Grant, B.J., and McCammon, J.A. (2008). Mapping the nucleotide and isoform-dependent structural and dynamical features of Ras proteins. Structure *16*, 885–896.

Grant, B.J., Gorfe, A.A., and McCammon, J.A. (2009). Ras conformational switching: simulating nucleotide-dependent conformational transitions with accelerated molecular dynamics. PLoS Comput. Biol. *5*, e1000325.

Grant, B.J., McCammon, J.A., and Gorfe, A.A. (2010). Conformational selection in g-proteins: lessons from ras and rho. Biophys. J. *99*, L87–L89.

Greasley, S.E., Jhoti, H., Teahan, C., Solari, R., Fensome, A., Thomas, G.M., Cockcroft, S., and Bax, B. (1995). The structure of rat ADP-ribosylation factor-1 (ARF-1) complexed to GDP determined from two different crystal forms. Nat. Struct. Biol. *2*, 797–806.

Güntert, P., Mumenthaler, C., and Wüthrich, K. (1997). Torsion angle dynamics for NMR structure calculation with the new program DYANA. J. Mol. Biol. *273*, 283–298.

Hall, B.E., Bar-Sagi, D., and Nassar, N. (2002). The structural basis for the transition from Ras-GTP to Ras-GDP. Proc. Natl. Acad. Sci. USA *99*, 12138–12142.

Hansen, D.F., Vallurupalli, P., and Kay, L.E. (2008). An improved ^{15}N relaxation dispersion experiment for the measurement of millisecond time-scale dynamics in proteins. J. Phys. Chem. B *112*, 5898–5904.

Henzler-Wildman, K., and Kern, D. (2007). Dynamic personalities of proteins. Nature *450*, 964–972.

Herrmann, T., Güntert, P., and Wüthrich, K. (2002). Protein NMR structure determination with automated NOE assignment using the new software CANDID and the torsion angle dynamics algorithm DYANA. J. Mol. Biol. *319*, 209–227.

Hillig, R.C., Hanzal-Bayer, M., Linari, M., Becker, J., Wittinghofer, A., and Renault, L. (2000). Structural and biochemical properties show ARL3-GDP as a distinct GTP binding protein. Structure *8*, 1239–1245.

Jaffe, A.B., and Hall, A. (2005). Rho GTPases: biochemistry and biology. Annu. Rev. Cell Dev. Biol. *21*, 247–269.

Kahn, R.A., Randazzo, P., Serafini, T., Weiss, O., Rulka, C., Clark, J., Amherdt, M., Roller, P., Orci, L., and Rothman, J.E. (1992). The amino terminus of ADP-ribosylation factor (ARF) is a critical determinant of ARF activities and is a potent and specific inhibitor of protein transport. J. Biol. Chem. *267*, 13039–13046.

Kahn, R.A., Volpicelli-Daley, L., Bowzard, B., Shrivastava-Ranjan, P., Li, Y., Zhou, C., and Cunningham, L. (2005). Arf family GTPases: roles in membrane traffic and microtubule dynamics. Biochem. Soc. Trans. *33*, 1269–1272.

Kahn, R.A., Cherfils, J., Elias, M., Lovering, R.C., Munro, S., and Schurmann, A. (2006). Nomenclature for the human Arf family of GTP-binding proteins: ARF, ARL, and SAR proteins. J. Cell Biol. *172*, 645–650.

Koshland, D.E. (1958). Application of a theory of enzyme specificity to protein synthesis. Proc. Natl. Acad. Sci. USA *44*, 98–104.

Laidler, K.J., and King, M.C. (1983). Development of transition-state theory. J. Phys. Chem. *87*, 2657–2664.

Li, Y., Kelly, W.G., Logsdon, J.M., Schurko, A.M., Harfe, B.D., Hill-Harfe, K.L., and Kahn, R.A. (2004). Functional genomic analysis of the ADP-ribosylation factor family of GTPases: phylogeny among diverse eukaryotes and function in C. elegans. FASEB J. *18*, 1834–1850.

Liu, Y., Kahn, R.A., and Prestegard, J.H. (2009). Structure and membrane interaction of myristoylated ARF1. Structure *17*, 79–87.

Liu, Y., Kahn, R.A., and Prestegard, J.H. (2010). Dynamic structure of membrane-anchored Arf·GTP. Nat. Struct. Mol. Biol. *17*, 876–881.

Loria, J.P., Rance, M., and Palmer, A.G., III. (1999). A relaxation-compensated Carr–Purcell–Meiboom–Gill sequence for characterizing chemical exchange by NMR spectroscopy. J. Am. Chem. Soc. *121*, 2331–2332.

Luz, Z., and Meiboom, S. (1963). Nuclear magnetic resonance study of the protolysis of trimethylammonium ion in aqueous solution—order of the reaction with respect to solvent. J. Chem. Phys. *39*, 366–370.

Ma, J., and Karplus, M. (1997). Molecular switch in signal transduction: reaction paths of the conformational changes in ras p21. Proc. Natl. Acad. Sci. USA *94*, 11905–11910.

Ma, B., Kumar, S., Tsai, C.J., and Nussinov, R. (1999). Folding funnels and binding mechanisms. Protein Eng. *12*, 713–720.

Mossessova, E., Corpina, R.A., and Goldberg, J. (2003). Crystal structure of ARF1·Sec7 complexed with Brefeldin A and its implications for the guanine nucleotide exchange mechanism. Mol. Cell *12*, 1403–1411.

Mulder, F.A., Mittermaier, A., Hon, B., Dahlquist, F.W., and Kay, L.E. (2001). Studying excited states of proteins by NMR spectroscopy. Nat. Struct. Biol. *8*, 932–935.

Ménétrey, J., Macia, E., Pasqualato, S., Franco, M., and Cherfils, J. (2000). Structure of Arf6-GDP suggests a basis for guanine nucleotide exchange factors specificity. Nat. Struct. Biol. *7*, 466–469.

Noé, F., Ille, F., Smith, J.C., and Fischer, S. (2005). Automated computation of low-energy pathways for complex rearrangements in proteins: application to the conformational switch of Ras p21. Proteins *59*, 534–544.

Paris, S., Béraud-Dufour, S., Robineau, S., Bigay, J., Antonny, B., Chabre, M., and Chardin, P. (1997). Role of protein-phospholipid interactions in the activation of ARF1 by the guanine nucleotide exchange factor Arno. J. Biol. Chem. *272*, 22221–22226.

Pasqualato, S., Renault, L., and Cherfils, J. (2002). Arf, Arl, Arp and Sar proteins: a family of GTP-binding proteins with a structural device for "front-back" communication. EMBO Rep. *3*, 1035–1041.

Peyroche, A., Antonny, B., Robineau, S., Acker, J., Cherfils, J., and Jackson, C.L. (1999). Brefeldin A acts to stabilize an abortive ARF-GDP-Sec7 domain protein complex: involvement of specific residues of the Sec7 domain. Mol. Cell *3*, 275–285.

Randazzo, P.A., Terui, T., Sturch, S., and Kahn, R.A. (1994). The amino terminus of ADP-ribosylation factor (ARF) 1 is essential for interaction with Gs and ARF GTPase-activating protein. J. Biol. Chem. *269*, 29490–29494.

Randazzo, P.A., Terui, T., Sturch, S., Fales, H.M., Ferrige, A.G., and Kahn, R.A. (1995). The myristoylated amino terminus of ADP-ribosylation factor 1 is a phospholipid- and GTP-sensitive switch. J. Biol. Chem. *270*, 14809–14815.

Renault, L., Guibert, B., and Cherfils, J. (2003). Structural snapshots of the mechanism and inhibition of a guanine nucleotide exchange factor. Nature *426*, 525–530.

Sali, A., and Blundell, T.L. (1993). Comparative protein modelling by satisfaction of spatial restraints. J. Mol. Biol. *234*, 779–815.

Shiba, T., Kawasaki, M., Takatsu, H., Nogi, T., Matsugaki, N., Igarashi, N., Suzuki, M., Kato, R., Nakayama, K., and Wakatsuki, S. (2003). Molecular mechanism of membrane recruitment of GGA by ARF in lysosomal protein transport. Nat. Struct. Biol. *10*, 386–393.

Spoerner, M., Herrmann, C., Vetter, I.R., Kalbitzer, H.R., and Wittinghofer, A. (2001). Dynamic properties of the Ras switch I region and its importance for binding to effectors. Proc. Natl. Acad. Sci. USA *98*, 4944–4949.

Spoerner, M., Wittinghofer, A., and Kalbitzer, H.R. (2004). Perturbation of the conformational equilibria in Ras by selective mutations as studied by ^{31}P NMR spectroscopy. FEBS Lett. *578*, 305–310.

Spoerner, M., Nuehs, A., Herrmann, C., Steiner, G., and Kalbitzer, H.R. (2007). Slow conformational dynamics of the guanine nucleotide-binding protein Ras complexed with the GTP analogue GTPγS. FEBS J. *274*, 1419–1433.

Spoerner, M., Hozsa, C., Poetzl, J.A., Reiss, K., Ganser, P., Geyer, M., and Kalbitzer, H.R. (2010). Conformational states of human rat sarcoma (Ras) protein complexed with its natural ligand GTP and their role for effector interaction and GTP hydrolysis. J. Biol. Chem. *285*, 39768–39778.

Stenmark, H. (2009). Rab GTPases as coordinators of vesicle traffic. Nat. Rev. Mol. Cell Biol. *10*, 513–525.

Vetter, I.R., and Wittinghofer, A. (2001). The guanine nucleotide-binding switch in three dimensions. Science *294*, 1299–1304.

Wennerberg, K., Rossman, K.L., and Der, C.J. (2005). The Ras superfamily at a glance. J. Cell Sci. *118*, 843–846.

